J. Phys. Soc. Jpn.
Downloaded from journals.jps.jp by 45.90.208.245 on 07/24/22

Journal of the Physical Society of Japan **91**, 084002 (2022)
https://doi.org/10.7566/JPSJ.91.084002

The Double-Peak Specific Heat in the Two Dimensional J_1–J_2 3-State Clock Model

Xue-Kai Ma and Li-Ping Yang*

Department of Physics, Chongqing University, Chongqing 401331, China

(Received May 19, 2021; accepted June 20, 2022; published online July 21, 2022)

By the extensive tensor network algorithms, the J_1–J_2 3-state clock model is investigated. We focus on the case of $J_1 > 0$, $J_2 < 0$, in which the double-peak structure appears in the curve of the specific heat C_v versus the temperature T. The four parameters $J_2 = -0.2, -0.8, -1.4, -2$ are chosen for the detailed numerical simulation in unit of $J_1 = 1$. The mismatch of peak position between entanglement entropy (EE) and C_v suggests the existence of two Berezinskii–Kosterlitz–Thouless (BKT) phase transitions in case of $J_2 = -0.2, -0.8$, where the peaks of EE lie inbetween the double peaks of C_v. In the case of $J_2 = -1.4$, the first-peak temperature of C_v and of EE are very close. With further increasing of $|J_2|$, the sequence of the first peak swaps, i.e., the first peak of EE arises at a lower temperature than of C_v. We believe that there is a critical $|J_2|$, above which the first peak of C_v does not correspond to the BKT phase transition. The location offset of the second peak between EE and C_v becomes smaller with $|J_2|$ increasing. In addition, the double-peak structure of the specific heat still holds when $|J_2|$ is large enough.

1. Introduction

Onsager's rigorous solution[1] of the two-dimensional Ising model provided the deep insight about the phase transition. The q-state clock model or Potts model are the natural generalization of Ising model. q optional spin states at each site enrich the phase transition greatly. In the case of $q = 2$, it is exactly Ising model demonstrating the phase transition driven by the symmetry breaking, being of Landau–Ginzburg type.[2] When $q > 4$[3] on the square lattice, the ferromagnetic clock system experiences two BKT[4,5] transitions exihibiting the topological feature, beyond Landau's paradigm.

Besides the nearest-neighbor (NN) interaction, the introduction of the next-nearest-neighbor (NNN) interaction diversifies the above general Ising model further. The competition between the configuration entropy, especially due to the interplay of the NN and NNN interactions, and the internal energy renders the rich phase diagram.

In this article, we will address the J_1–J_2 3-state clock model, and the Hamiltonian reads as

$$H = J_1 \sum_{\langle ij \rangle} \cos\theta_{ij} + J_2 \sum_{\langle\langle ij \rangle\rangle} \cos\theta_{ij}. \tag{1}$$

Here, $\theta_{ij} \equiv \theta_i - \theta_j$, and J_1, J_2 refer to the coupling strength inbetween the NN pair, and the NNN pair, respectively. At each site $\theta_i = 2\pi k_i/3$, with $k_i = 0, 1, 2$.

In what follows, we will focus on the case of $J_1 > 0$, $J_2 < 0$. For convenience, J_1 is set as 1 favoring the super anti-ferromagnetic (AF) order in NN pair. To be specific, the NN pair tends to take the different k. There are three combinations: $(01, 12, 02)$, in which the energy from the NN bond is equivalent. The NNN pair favors the ferromagnetic alignment. Although the research is free from the frustration, there are strongly degenerate configurations. Figure 1 is the typical one with the super antiferromagnetic order, relevant to the broken-sublattice-symmetry (BSS) state:[6] one sublattice is broken into one spin state, and the other sublattice take the random distribution from the other two spin states.

In the case of $J_2 = 0$, the configuration shown in Fig. 1 corresponds to the ground state. Thus there exists the extensive entropy, i.e., $S = (1/2)\ln 2$. Our check on the specific heat and the entanglement entropy do not show any singularity in the finite temperature, conforming to the rigorous solution from Baxter.[7] Once the negative J_2 is switched on, no matter how small, in the low temperature limit, the option in the red circle will become unique other than the two possibilities ($k = 1, 2$) in Fig. 1. Negative J_2 will not induce any frustration for the super AF order that the positive J_1 favors. On the contrary, $J_2 < 0$ enhance the partial order as shown in Fig. 1. In the low temperature limit, we have the ground state energy $E_g = -J_1 + 2J_2$. In the high temperature limit, all the configurations share the same Boltzmann weight. As a result, the entropy per site S equals $\ln 3$.

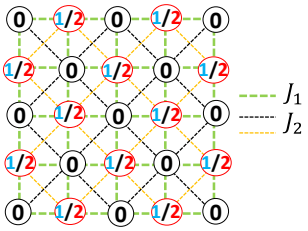

Fig. 1. (Color online) The configuration with the partial order. The option 0 form the stable stripe order along the black dash diagonal line, the sites along the adjacant diagonal line hold two possibilities, which renders $S = (1/2)\ln 2$.

The previous research about the J_1–J_2 3-state (Potts or clock) on the square lattice include the renormalization group treatment,[8–10] Monte-Carlo (MC) simulation[6,11–13] and level spectroscopy method.[14] First, the results from the renormalization group are as follow: Cardy[9] claimed the existence of two phase transitions with a critical line of continuously varying exponent η. den Nijs et al. demonstrated the critical fan with an infinite-order transition crossing the lower boundary into the disordered phase for some fixed parameters. Oliveira et al. showed the existence of the three fixed points separating the phase diagram into three regions: ferro-, antiferro-, and para-magnetic phases, and the system flows to antiferromagnetic or paramagnetic phase away from the semistable fixed point $(t_1^*, t_2^*) = (-0.375, 0.150)$ ($q = 3$ Potts). Second, concerning the numerical simulations, by MC, Grest et al. showed the two successive phase transitions: from AF to BSS phase, and to paramagnetic phase in high temperature, however, Ono claimed the occurence of

©2022 The Physical Society of Japan

J. Phys. Soc. Jpn.
Downloaded from journals.jps.jp by 45.90.208.245 on 07/24/22

Table I. Comparison of results in previous works.

References	Methods	Results
Cardy[9]	renormalization group	a sequence of two infinite-order BKT phase transitions
den Nijs et al.[10]	phenomelogical renormalization group	a critical fan in which the infinite-order phase transition occurs
Oliveira et al.[8]	real-space renormalization group	there exist three fixed points separating the phase diagram into three regions: ferro-, antiferro-, and para-magnetic phases
Grest and Banavar[6]	MC simulation	two phase transitions: successively from AF phase with sixfold degeneracy to BSS phase, and to paramagnetic phase in high temperature
Ono[11,12]	MC simulation	the occurrence of the BKT phase transition
Otsuka et al.[14]	dual sine-Gordon Lagrangian, level-spectroscopy method	There exists a critical region bounded by two BKT lines ending at $(J_1/T, J_2/T) = (0, \log(1+\sqrt{3}))$. The ordered phase lies above the upper BKT line, and the disordered phase lies below the lower BKT line

Berezinskii–Kosterlitz–Thouless (BKT) phase transitions by the estimation of the critical exponent η. Combining the level-spectroscopy method and transfer matrices, Otsuka et al. demonstrated the two BKT lines embracing a critical region, beyond which there are ordered (upward) and disordered (downward) phases respectively. The comparison about the methods and the main conclusions is listed in Table I. Most of the research suggested the BKT phase transition. Our recent research[3] by the tensor renormalization group[15] (TRG) provided exact and satisfactory results about the BKT criticality of two-dimensional q-state clock model. Hereafter, we adopt TRG to investigate this model. As far as we know, it is the first try.

For any classical statistical model with the local interactions, the partition function can be expressed as the contraction of the tensor network.[16] The tensor network algorithms bring the remarkable breakthrough in the numerical simulations, no matter whether in the intractable quantum spin liquid issue,[17,18] or in the spin class problem.[19] We exploit the relevant corner transfer matrix method[20–23] to calculate the physical observables: the free energy (F), energy (E), thermal entropy (S), the specific heat (C_v), and the local structure factor ($S_{\pi,\pi}$), which are used to explore the phase transition behaviors of the J_1–J_2 3-state model on the square lattice. In particular, we calculate the entanglement entropy (S_E) of the original and dual lattice. The comparison of the peak location inbetween C_v and S_E provide an extra perspective for the understanding for the phase transition.

The article is organized as follows. In Sect. 2, we introduce the tensor network and representations about the original and dual lattice, by which the physical observables are obtained. The temperature dependence of the double-peak specific heat and the observables are demonstrated and studied. By the entanglement spectrum of the converged matrix product state during the transfer matrix renormalization group, we calculate the entanglement entropy. The peak location of C_v and S_E are compared. Finally, we go to the conclusion in Sect. 3.

2. Numerical Results

The duality embedded in the construction of the transfer matrix[24] applys to our tensor initialization. The variables of the original lattice is the angle θ located on the lattice site, while the counterpart is the angle difference defined on the bond connecting the nearest neighbour pair (so called the dual lattice).[3,25]

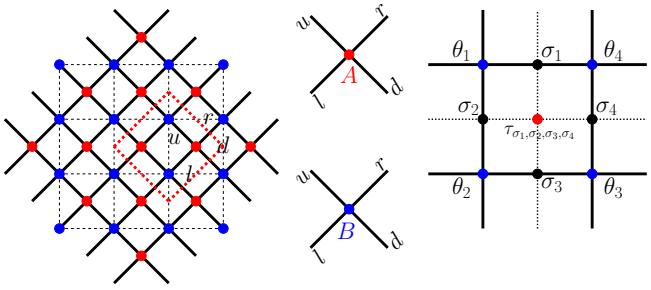

Fig. 2. (Color online) The tensor network and the related tensor representation (left panel). Two As and Bs form the the unit cell (enclosed by the red dash line); The dual lattice shown by dotted line with the tensor unit $\tau_{\sigma_1,\sigma_2,\sigma_3,\sigma_4}$ (right panel). Here, $\sigma_1 = \theta_1 - \theta_4$ along the anti-clockwise direction, and θs denote the angles of the original lattice sites.

First, in the original lattice, there are two types of tensor unit: A and B. As is shown in the left panel of Fig. 2, the whole tensor network exhibits the periodicity with the unit cell 2×2 (enclosed by the red dash line).[26] The partition function is expressed as

$$Z = \sum_{\{\theta\}} e^{-\beta H(\{\theta\})} = \mathrm{Tr}(\ldots ABBA \ldots), \tag{2}$$

where the sum takes over all configurations labelled by $\{\theta\}$, and the tensor A and B read as

$$\begin{aligned} A_{lrud} &= \exp[-\beta J_1(\cos\theta_{lu} + \cos\theta_{ur} + \cos\theta_{rd} + \cos\theta_{dl})/2] \\ &\quad \times \exp[-\beta J_2(\cos\theta_{lr} + \cos\theta_{ud})], \\ B_{lrud} &= \delta_{lrud} = \begin{cases} 1, & l = r = u = d \\ 0, & \text{others} \end{cases}. \end{aligned} \tag{3}$$

Here, l, r, u, d are the tensor indices emitting from the site A, B.

Second, the unit tensor in the dual lattice referring to the right panel of Fig. 2 is defined as

$$\begin{aligned} \tau_{\sigma_1,\sigma_2,\sigma_3,\sigma_4} &= \exp\{-\beta J_1(\cos\sigma_1 + \cos\sigma_2 + \cos\sigma_3 + \cos\sigma_4)/2 \\ &\quad + J_2(\cos(\sigma_1+\sigma_2) + \cos(\sigma_3+\sigma_4))\}. \end{aligned} \tag{4}$$

Here, σ_i equals the angle difference at two ends of the bond anticlockwise. The directional corner transfer matrix method[23] is used to contract the tensor network in the dual lattice. The corner transfer matrix renormalization group (CTMRG) algorithm[20–22] is applied to the original lattice network. The physical quantities can be calculated by the "impurity" method.[27]

©2022 The Physical Society of Japan

J. Phys. Soc. Jpn.
Downloaded from journals.jps.jp by 45.90.208.245 on 07/24/22

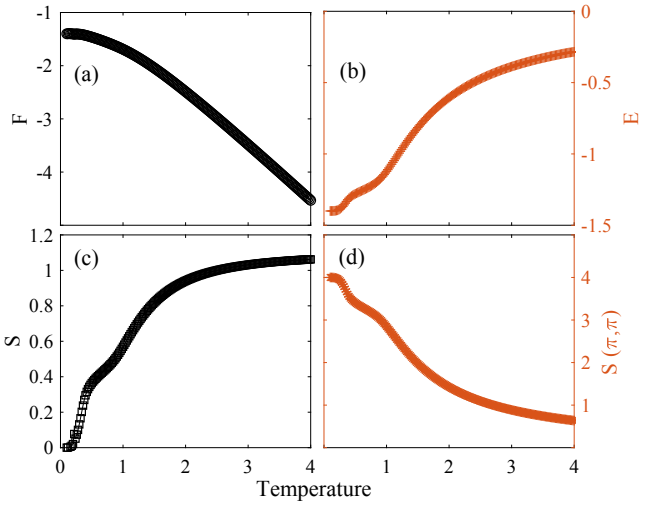

Fig. 3. (Color online) The temperature dependence of the physical quantities: the free energy (F), the internal energy (E), the thermal entropy (S), and the local structure factor $S_{(\pi,\pi)}$. Here, $J_2 = -0.2$, $D = 60$.

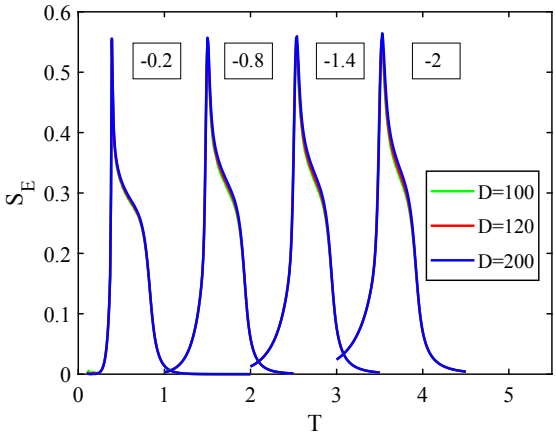

Fig. 5. (Color online) The temperature dependence of the entanglement entropy S_E in the cases with the different J_2 couplings. The different kept dimension $D = 100, 120, 200$ are compared from the dual lattice calculation, by which the low-temperature critical point is determined.

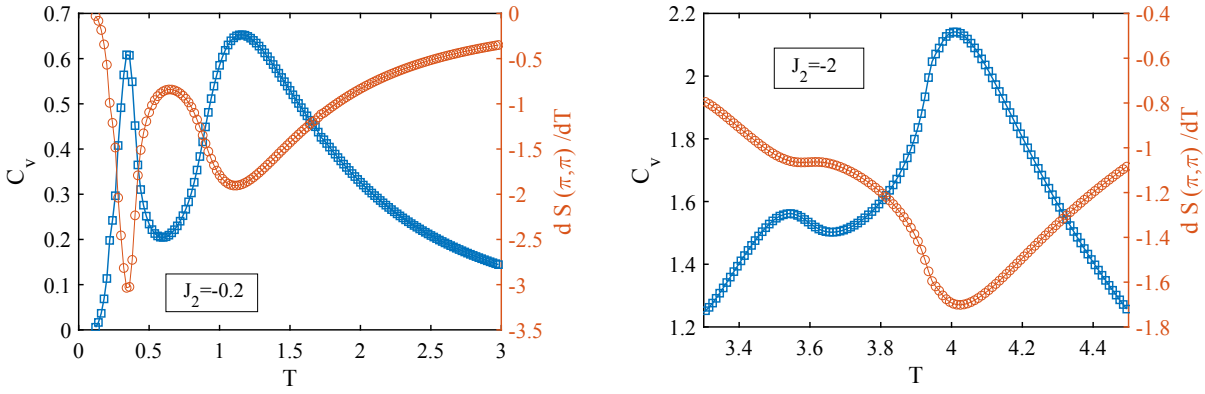

Fig. 4. (Color online) The comparison of the temperature dependence of the specific heat C_v (orange red circle) and the temperature gradient of the local structure factor $dS_{(\pi,\pi)}/dT$ (blue square) in the two cases: $J_2 = -0.2$ (left panel) and $J_2 = -2$ (right panel). Here, $D = 60$.

Utilizing the local unit cell in the original lattice, the structure factor is defined as

$$S_{\boldsymbol{q}} = \frac{1}{2}\sum_{m\neq n} \exp(i\boldsymbol{q}\cdot(\boldsymbol{r}_m - \boldsymbol{r}_n))\cos(\theta_m - \theta_n). \tag{5}$$

Here, $S_{\boldsymbol{q}}$ is not a global structure factor, but a local observable provided that the translational invariance is preserved. Here, $\boldsymbol{r}_m$ means the position vector of the m-th site in the unit cell $(m, n = 1, 2, 3, 4)$ and the prefactor $1/2$ is used to avoid the double counting. According to the definition of the magnetization M for the BSS state, M takes 1 for any configuration in Fig. 1, corresponding to the perfect partial order. $S_{(\pi,\pi)}$ can also be used to roughly observe the perfect partial order, and takes the maximum value 4 [see Fig. 3(d)] in the low temperature limit in case of $J_2 < 0$, referring to the configuration with one certain value out of $(1, 2)$ for the sites along the yellow dash diagonal lines as shown in Fig. 1.

In the meanwhile, the internal energy per site takes the minimum value $-J_1 + 2J_2$, i.e., $E_g = -1.4$ in the case of $J_2 = -0.2$. As is shown in Fig. 3, the free energy and $S_{(\pi,\pi)}$ decrease with the temperature increasing, and the internal energy and the entropy take the other way around. In the low temperature limit, the nonzero J_2 will break the extensive entropy. As a result, the entropy $S = 0$ holds, and the free energy is equivalent to the internal energy, i.e., $F = E = -1.4$.

Concerning the analytical similarity of the curves between the internal energy and $S_{(\pi,\pi)}$ versus the temperature, we take the derivative with respect to the temperature for the further observation. As is shown in Fig. 4, the singularity of C_v and $dS_{(\pi,\pi)}/dT$ are located at the same temperature.

Moreover, the entanglement entropy (EE) is found to be an effective signal to locate the phase transition.[28] By the EE, the critical temperatures of the BKT phase transition in clock-q model are accurately determined.[3] The Kramers–Wannier transformation[29] related to the duality leads to the exchange of the low and high temperature phases, due to which we calculate the EE in the original and dual lattice. The peaks of the EE help us to pin down the critical points.

Figure 5 demonstrates the singularities of the EE with different J_2 couplings. The different kept dimension $D = 100, 120, 200$ indicates the convergency. The peak location pins down the critical point in the low temperature from the dual lattice calculation. Combining the numerical simulations in the original lattice, the critical point in the high temperature is also determined. The critical temperatures are listed

©2022 The Physical Society of Japan

J. Phys. Soc. Jpn.
Downloaded from journals.jps.jp by 45.90.208.245 on 07/24/22

Table II. The temperature corresponding to the two peaks of the specific heat and the entanglement entropy in the cases of $J_2 = -0.2, -0.8, -1.4, -2$.

T / C_v, S_E / J_2	S_{E1}	C_{v1}	C_{v2}	S_{E2}
−0.2	0.3910(1)	0.3509(1)	1.1541(1)	0.8403(1)
−0.8	1.5035(1)	1.457(1)	2.0722(1)	1.9502(1)
−1.4	2.5359(1)	2.530(1)	3.044(1)	2.9601(1)
−2	3.5300(1)	3.530(1)	4.009(1)	3.9501(1)

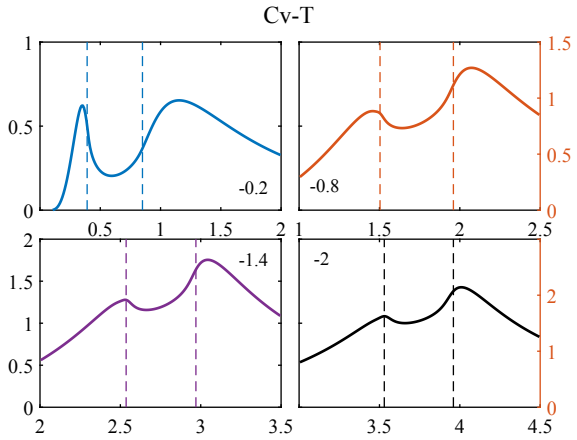

Fig. 6. (Color online) The comparison of the temperature dependence of the specific heat in the cases with the different J_2 couplings by the dual lattice calculation with $D = 200$. The two vertical lines mean the peak locations of the entanglement entropy from the dual (left dash line) and original (right dash line) lattice, respectively. Here, $J_1 = 1$, and $J_2 = -0.2, -0.8, -1.4, -2$, respectively.

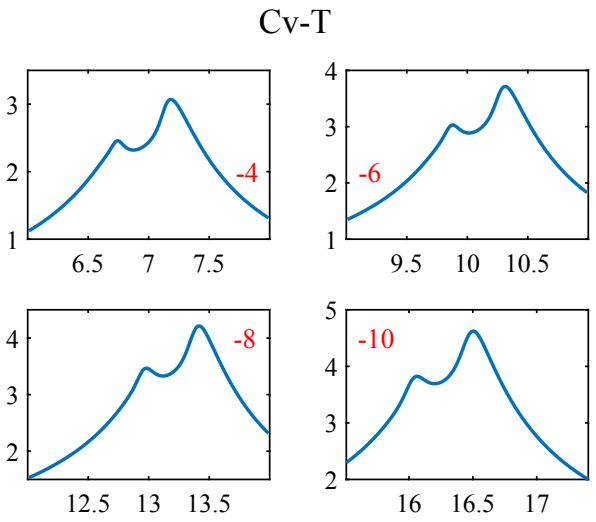

Fig. 7. (Color online) The temperature dependence of the specific heat C_v when $|J_2|$ increases further: $J_2 = -4, -6, -8, -10$, respectively. The calculation is from the dual lattice with $D = 200$.

in Table II, in which the middle two columns refer to the peak location of C_v. As is shown in the upper panel of Fig. 6, the peaks of the S_E lie in between the peaks of C_v, which is a typical characteristic of the BKT phase transition. Referring to the data in Table II, we find that the case of $J_2 = -0.2$ lies in the critical region in the phase diagram in Ref. 14, however, $J_2 = -0.8$ case lies below and close to the lower BKT boundary line. The cases of $J_2 = -1.4, -2$ are further away from the lower BKT boundary line and lie in the disordered region in Fig. 2 of Ref. 14. Our numerical simulations suggest a higher upper limit of $|J_2|$ for the occurrence of the BKT phase transition in unit of $J_1 = 1$.

In the sense of the partial order, $J_1 = 1$ favors the super anti-ferromagnetic configuration in the NN pair. Nonzero J_2 induces the double-peak structure in the specific heat, as shown in Fig. 6. With $|J_2|$ increasing, the peaks shift towards the high temperature. In the limit $|J_2| \to \infty$, the system is decoupled into two ferromagnetic clock-3 model, same to the case with $J_1 = -1$, $J_2 = 0$, where the rigorous critical temperature $T_c = 3/(2\ln(\sqrt{3}+1)) \approx 1.49246$. The rigorous value can be obtained by the duality from the transfer matrix treatment,[24,30] or from the tensor construction of the original and dual lattice.[25]

Do the two peaks meet[11] each other finally? We further calculate more cases with larger $|J_2| = 4, 6, 8, 10$. The double-peak structure of C_v still holds, as shown in Fig. 7. Unexpectedly the temperature difference of the two peaks even does not change significantly with $|J_2|$ increasing. Thus we do not think that the two peaks will merge at finitely large $|J_2|$. Once $|J_2|$ goes to infinity, the system is decoupled to two independent ferromagnetic clock-3 model. The scaled critical temperature $T_c/|J_2|$ in case of $|J_2| = 10$ is close to the exact value mentioned above. Note that the fist peak of S_E occurs at a lower temperature compared to C_v in these large $|J_2|$ cases. It indicates that there is a change about the phase nature when $|J_2|$ increases further. The more research is needed for the observation.

3. Conclusion

In summary, we investigate the partial order in the classical J_1–J_2 clock-3 model. $J_1 > 0$ favors the situation that the NN pair takes different k. In the low temperature regime, $J_2 < 0$ lock down the order in the black square shown in Fig. 1. $S_{\pi,\pi}$ is the local structure factor for observing the partial order, and we find that $dS_{\pi,\pi}/dT$ and C_v keep similar singularity.

There exhibits the double-peak structure in the specific heat. For the small $|J_2|$, we check the partial order at low temperature region. By the calculation from the original and dual lattice, the critical points are accurately determined by the singularity of the entanglement entropy. The numerical data is listed in Table II. The mismatch, with two peaks of S_E lie between the two peaks of C_v, suggests the BKT phase transition. The first peak of S_E becomes to lie before the first peak of C_v with $|J_2|$ increasing, which indicates the change of the phase transition nature.

For the larger $|J_2|$, the singularity of the C_v curve moves to the higher temperature. In our calculation, the double peak structure of C_v still holds when $|J_2| = 10$. The temperature difference of the two C_v peaks keeps almost unchanged with $|J_2|$ increasing, not even in the sense of the unit scaled by $|J_2|$.

However, limited to the precision of the numerical simulations in the neighborhood of the critical points, the scaling analysis is absent, as a result, we have not determined the critical exponent. The strongly degenerated configurations bring the instability in the numerical simulation. As we observe, the sequence swap of the first peak of S_E and of C_v indicates the existence of the upper limit of $|J_2|$ for the BKT phase transition. Then what are the upper and lower critical values of $|J_2|$ as concerns the low temperature BKT phase

©2022 The Physical Society of Japan

J. Phys. Soc. Jpn.
Downloaded from journals.jps.jp by 45.90.208.245 on 07/24/22

transition? It is on the way for the further exploration, including but not limited to: the larger D, the crosscheck with the other tensor algorithms, and the extraction of the criticality and university.[3,26)]

Acknowledgments We appreciate the stimulating suggestion from Xue-Feng Zhang, and helpful discussion with Cheng-Xiang Ding. This work is supported by National Science Fundation of China, NSFC (Grant No. 11874095), National Science Fundation of Chongqing (Grant No. cstc2018jcyjAX0399), and Research Funds for the Central Universities (No. 2018CDXYWU0025).

*liping2012@cqu.edu.cn

1) L. Onsager, Phys. Rev. **65**, 117 (1944).
2) L. D. Landau, E. M. Lifshitz, and E. M. Pitaevskii, *Statistical Physics* (Butterworth-Heinemann, New York, 1999).
3) Z.-Q. Li, L.-P. Yang, Z. Y. Xie, H.-H. Tu, H.-J. Liao, and T. Xiang, Phys. Rev. E **101**, 060105(R) (2020).
4) V. L. Berezinskii, Sov. Phys. JETP **32**, 493 (1971).
5) J. M. Kosterlitz and D. J. Thouless, J. Phys. C **5**, L124 (1972); J. M. Kosterlitz and D. J. Thouless, J. Phys. C **6**, 1181 (1973).
6) G. S. Grest and J. R. Banavar, Phys. Rev. Lett. **46**, 1458 (1981).
7) R. J. Baxter, Proc. R. Soc. London, Ser. A **383**, 43 (1982).
8) P. M. Oliveira, C. Tsallis, and G. Schwachheim, Phys. Rev. B **29**, 2755 (1984).
9) J. L. Cardy, Phys. Rev. B **24**, 5128 (1981).
10) M. P. M. den Nijs, M. P. Nightingale, and M. Schick, Phys. Rev. B **26**, 2490 (1982).
11) I. Ono, J. Phys. Soc. Jpn. **53**, 4102 (1984).
12) I. Ono and A. Yamagata, J. Magn. Magn. Mater. **90–91**, 309 (1990).
13) Y. Okabe and H. Otsuka, J. Phys. A **39**, 9093 (2006).
14) H. Otsuka, K. Mori, and Y. Okabe, Phys. Rev. E **72**, 046103 (2005).
15) M. Levin and C. P. Nave, Phys. Rev. Lett. **99**, 120601 (2007).
16) H. H. Zhao, Z. Y. Xie, Q. N. Chen, Z. C. Wei, J. W. Cai, and T. Xiang, Phys. Rev. B **81**, 174411 (2010).
17) Z. Y. Xie, J. Chen, J. F. Yu, X. Kong, B. Normand, and T. Xiang, Phys. Rev. X **4**, 011025 (2014).
18) H. J. Liao, Z. Y. Xie, J. Chen, Z. Y. Liu, H. D. Xie, R. Z. Huang, B. Normand, and T. Xiang, Phys. Rev. Lett. **118**, 137202 (2017).
19) C. Wang, S.-M. Qin, and H.-J. Zhou, Phys. Rev. B **90**, 174201 (2014).
20) T. Nishino, K. Okunishi, Y. Hieida, N. Maeshima, and Y. Akutsu, Nucl. Phys. B **575**, 504 (2000).
21) T. Nishino, Y. Hieida, K. Okunishi, N. Maeshima, Y. Akutsu, and A. Gendiar, Prog. Theor. Phys. **105**, 409 (2001).
22) P. Corboz, J. Jordan, and G. Vidal, Phys. Rev. B **82**, 245119 (2010).
23) R. Orús and G. Vidal, Phys. Rev. B **80**, 094403 (2009).
24) G. Ortiz, E. Cobanera, and Z. Nussinov, Nucl. Phys. B **854**, 780 (2012).
25) J. Chen, H.-J. Liao, H.-D. Xie, X.-J. Han, R.-Z. Huang, S. Cheng, Z.-C. Wei, Z.-Y. Xie, and T. Xiang, Chin. Phys. Lett. **34**, 050503 (2017).
26) H. Li and L.-P. Yang, Phys. Rev. E **104**, 024118 (2021).
27) H.-H Zhao, Z.-Y. Xie, T. Xiang, and M. Imada, Phys. Rev. B **93**, 125115 (2016).
28) R. Krčmár, A. Gendiar, and T. Nishino, arXiv:1612.07611.
29) H. A. Kramers and G. H. Wannier, Phys. Rev. **60**, 252 (1941).
30) H. Kramers and G. Wannier, Phys. Rev. **60**, 252 (1941).

©2022 The Physical Society of Japan